ECCOMAS Congress 2016
VII European Congress on Computational Methods in Applied Sciences and Engineering
M. Papadrakakis, V. Papadopoulos, G. Stefanou, V. Plevris (eds.)
Crete Island, Greece, 5–10 June 2016

THERMOMECHANICAL NUMERICAL SIMULATION OF IMPACTS ON ELASTIC-PLASTIC SOLIDS WITH THE FINITE VOLUME METHOD

Thomas Heuzé[1]

[1]Research Institute in Civil and Mechanical Engineering (GeM, UMR 6183 CNRS)
École Centrale de Nantes, 1 rue de la Noë, F-44321 Nantes, France
e-mail: thomas.heuze@ec-nantes.fr

Keywords: Thermomechanics, Finite volume method, Impacts, Thermo-elastic-plastic solids.

Abstract. *We present in this work two implementation schemes of the finite volume method for the numerical simulation of impacts on thermo-elastic-plastic solids within the small strain framework for one dimension (bar) solid media, based on the Lax-Wendroff and high (second) order TVD methods. A strong thermomechanical coupling and adiabatic conditions are assumed. Comparison is performed with results obtained with the classical finite element method and an analytical solution on a test case involving a discontinuous solution. The finite volume methods (mainly the high order TVD one) improve both the track of the shock wave path, even after many reflexions of waves, and the computation of plastic strains and temperature.*

1 INTRODUCTION

The modelling and numerical simulation of hyperbolic initial boundary value problems including extreme loading conditions such as impacts require the ability to accurately capture and track the wave front of shock waves induced in the medium. Indeed, this permits to both understand correctly the path of waves and assess accurately the field of plastic strains and hence that of residual stresses within a structure. These problems require therefore numerical schemes able to meet high orders of accuracy and a high resolution of discontinuity without any spurious oscillations.

The numerical simulation of impacts on dissipative solids has been and is again mainly performed with the classical finite element method implemented in many industrial codes. However, finite elements do not use any feature of the characteristic structure of the set of hyperbolic equations, and the amount of artificial viscosity added to numerical time integrators is hard to assess properly in order to remove the sole spurious oscillations. Hence, a poor resolution of discontinuity and track of the wave path is generally achieved.

The finite volume method, initially developed for the simulation of gas dynamics [1], has gained recently more and more interest for problems involving impacts on solid media. The characteristic structure of the set of hyperbolic equations can be accounted for by the solution of a Riemann problem at interfaces between cells, and the same order of convergence is achieved for both the displacement and stress fields [2]. Several authors [3, 4, 5, 6, 7] have proposed many ways to simulate impacts on dissipative solid media such that elastic-plastic solids.

In this work, we use the finite volume method for the numerical simulation of impacts on thermo-elastic-plastic solids within the small strain framework in one dimension (actually bars here), and compare it to results obtained with the classical finite element method. First, the set of equations considered are presented in section 2. Since the material is deformed at high strain rate, adiabatic conditions are assumed to compute the rise of temperature, and the thermal softening is accounted for. Next, two implementations schemes of the finite volume method for this kind of material are presented in section 3: the Lax-Wendroff method and a high-order TVD method using the Superbee limiter. Then, the finite volumes numerical solutions are compared to the results of the finite element method and to an analytical solution of a test case involving a discontinuous solution in section 4.

2 INITIAL BOUNDARY VALUE PROBLEM FOR A THERMO-ELASTIC-PLASTIC MATERIAL IN ONE DIMENSION

We consider in this work a unidimensional initial boundary value problem written for a thermo-elastic-plastic material within the linearized small strain framework. The set of conservation laws reads:

$$\frac{\partial \mathbf{u}}{\partial t} + \frac{\partial \mathbf{f}(\mathbf{u})}{\partial x} = \mathbf{0} \quad \forall x \in]0, L[\tag{1}$$

within a domain of length L, the unknown vector $\mathbf{u}$ and the flux $\mathbf{f}(\mathbf{u})$ are defined as

$$\mathbf{u} = \begin{bmatrix} \sigma \\ v \end{bmatrix} \; ; \quad \mathbf{f} = \begin{bmatrix} -Hv \\ -\sigma/\rho \end{bmatrix} \tag{2}$$

where ρ is the mass density, and σ and v denote the axial stress and velocity components respectively. The conservations laws (1) should be supplemented with appropriate boundary and initial conditions. For a purely elastic material, the modulus H is equal to the Young's modulus

E. For an elastic-plastic material, the modulus H stands for the tangent modulus:

$$\frac{d\sigma}{d\varepsilon} = \frac{EQ}{E+Q} \tag{3}$$

In this work, an elastic-plastic material with a linear isotropic material is considered. Moreover, the influence of the thermal part on the mechanical part is accounted for through thermal softening via a linear decrease of the tensile yield stress with the temperature. The constitutive set of equations are listed below:

$$\dot{\varepsilon} = \dot{\varepsilon}^e + \dot{\varepsilon}^p \tag{4}$$

$$\dot{\sigma} = E\dot{\varepsilon}^e \tag{5}$$

$$\dot{\varepsilon}^p = \dot{p}\ \text{sign}(\sigma) \tag{6}$$

$$f = |\sigma| - (\sigma_0 + Qp)\left(1 - A\frac{(T-T_0)}{T_0}\right) \leq 0 \tag{7}$$

$$\dot{p} \geq 0;\ f \leq 0; f\dot{p} = 0 \tag{8}$$

where the equations (4), (5), (6), (7) and (8) refer to the additive partition of the total strain rate ($\dot{\varepsilon}$) into elastic ($\dot{\varepsilon}^e$) and plastic ($\dot{\varepsilon}^p$) parts, the elastic law, the plastic flow rule, the criterion and the Kuhn-Tucker complementary conditions. In (6), $\dot{p}$ denotes the rate of cumulated plastic strain. The tensile yield stress in (7) involve the initial tensile yield stress σ_0, a strain hardening modulus Q, a decrease coefficient A and the reference temperature T_0. The temperature is solution of the heat equation, assuming adiabatic conditions, written with the sole mechanical dissipation on the right hand side:

$$\rho C\dot{T} = \sigma\dot{\varepsilon}^p - Qp\dot{p} \tag{9}$$

where C is the thermal heat capacity.

3 FINITE VOLUME METHODS

The finite volume methods are based on subdividing the spatial domain into grid cells [1] of length Δx, and defining the approximation $\mathbf{U}_i$ of $\mathbf{u}$ within the i^{th} grid cell by integral averaging. These are then updated using the conservation laws (2) written in integral form on one cell, generally coupled with an explicit time integration scheme. We present here the application of the Lax-Wendroff method and a high-order Total Variation Diminishing (TVD) method using the Superbee limiter, to a thermo-elastic-plastic material.

3.1 LAX-WENDROFF

The Lax-Wendroff method is a second order accurate method, presented here in its Richtmyer two-steps version. The first step amounts to approximate $\mathbf{u}$ at the midpoint in time $t_{n+1/2} = t_n + \Delta t/2$ (n referring to the time step number) by:

$$\mathbf{U}_{i+\frac{1}{2}}^{n+\frac{1}{2}} = \frac{\mathbf{U}_i^n + \mathbf{U}_{i+1}^n}{2} + \frac{\Delta t}{2\Delta x}(\mathbf{F}_i^n - \mathbf{F}_{i+1}^n) \tag{10}$$

The second step requires to evaluate the flux at this point

$$\mathbf{F}_{i+\frac{1}{2}}^n = \mathbf{f}\left(\mathbf{U}_{i+\frac{1}{2}}^{n+\frac{1}{2}}\right) \tag{11}$$

in order to update the unknowns at time t_{n+1} with the following conservative scheme:

$$\mathbf{U}_i^{n+1} = \mathbf{U}_i^n - \frac{\Delta t}{\Delta x}\left(\mathbf{F}_{i+\frac{1}{2}}^n - \mathbf{F}_{i-\frac{1}{2}}^n\right) \tag{12}$$

For implementing a thermo-elastic-plastic material, a dedicated Riemann solver should be considered. First, at each step of the Richtmyer algorithm, a prediction-correction scheme should be set in order to handle the Kuhn-Tucker complementary conditions (8). An elastic constitutive behaviour is first assumed, leading to an elastic trial solution. For the first Richtmyer step, it comes:

$$\left(\sigma_{i+\frac{1}{2}}^{n+\frac{1}{2}}\right)^{\text{trial}} = \frac{\sigma_i^n + \sigma_{i+1}^n}{2} + \frac{c_e^2 \Delta t}{2\Delta x}(\rho v_{i+1}^n - \rho v_i^n) \tag{13}$$

$$v_{i+\frac{1}{2}}^{n+\frac{1}{2}} = \frac{v_i^n + v_{i+1}^n}{2} + \frac{\Delta t}{2\Delta x}\left(\frac{\sigma_{i+1}^n - \sigma_i^n}{\rho}\right) \tag{14}$$

where c_e stands for the elastic sound speed defined by $c_e = \sqrt{E/\rho}$, generally set to $\Delta t/\Delta x$ if the Courant number is set at one. Then, the criterion (7) is computed with that trial state within the grid cells i and $i+1$, provided their respective cumulated plastic strain values p_i^n and p_{i+1}^n and temperature values T_i^n and T_{i+1}^n at time t_n. Two cases thus arise for each grid cell: either the plastic criterion is satisfied, and hence the evolution is actually elastic $\sigma_{i+1/2}^{n+1/2} = \left(\sigma_{i+1/2}^{n+1/2}\right)^{\text{trial}}$, or the plastic criterion is violated $f\left(\left(\sigma_{i+1/2}^{n+1/2}\right)^{\text{trial}}\right) > 0$, and a plastic correction needs to be carried out. In the latter case, the plastically admissible stress state should be computed by matching the elastic-plastic Riemann invariants defined on the two integral curves passing by the states of the grid cells i and $i+1$ at time t_n:

$$v_{i+\frac{1}{2}}^{n+\frac{1}{2}} = v_i^n + \frac{\Delta x}{\Delta t}\left(\int_{\sigma_i^n}^{\sigma_i^*} \frac{d\sigma}{\rho c^2} + \int_{\sigma_i^*}^{\sigma_{i+\frac{1}{2}}^{n+\frac{1}{2}}} \frac{d\sigma}{\rho c^2}\right) \tag{15}$$

$$v_{i+\frac{1}{2}}^{n+\frac{1}{2}} = v_{i+1}^n - \frac{\Delta x}{\Delta t}\left(\int_{\sigma_{i+1}^n}^{\sigma_{i+1}^*} \frac{d\sigma}{\rho c^2} + \int_{\sigma_{i+1}^*}^{\sigma_{i+\frac{1}{2}}^{n+\frac{1}{2}}} \frac{d\sigma}{\rho c^2}\right) \tag{16}$$

where σ_i^* and σ_{i+1}^* stand for the tensile yield stress in each grid cell at time t_n if the trial state did not satisfy the plastic criterion, or are equal to σ_i^n (resp. σ_{i+1}^n) if the plastic criterion has been satisfied. At one cell interface $i+1/2$, the plasticity can develop from its left side, from its right side, or from both. Hence the stress at this interface is updated based on the criterion assessed at the two grid cells:

$$\sigma_{i+\frac{1}{2}}^{n+\frac{1}{2}} = \frac{1}{\frac{1}{\rho c_i^2} + \frac{1}{\rho c_{i+1}^2}}\left(\frac{\sigma_i^*}{\rho c_i^2} + \frac{\sigma_{i+1}^*}{\rho c_{i+1}^2} + \frac{1}{\rho c_e^2}(\sigma_i^n + \sigma_{i+1}^n - \sigma_i^* - \sigma_{i+1}^*) + \frac{\Delta t}{\Delta x}(v_{i+1}^n - v_i^n)\right) \tag{17}$$

where c_i and c_{i+1} denote the sound speed at grid cell i and $i+1$. These are equal to c_e if the evolution is elastic, or c_p the plastic sound speed ($= \sqrt{(d\sigma/d\varepsilon)/\rho}$) if the evolution is elastic-plastic. The second step of the Richtmyer algorithm is also based on a prediction-correction scheme; the trial state is obtained via the conservative formula (12). This trial state is also tested with the plastic criterion within each grid cell provided its cumulated plastic strain value

p_i^n and temperature value T_i^n, and the same reasoning is applied. Once the stress have been updated at time t_{n+1}, the cumulated plastic strain are updated using the criterion (7), and hence the plastic strains through the plastic flow rule (6). The temperature is updated at the end of the time step through an implicit time discretization of (9):

$$T_i^{n+1} = T_i^n + \frac{1}{\rho C}(\sigma_i^{n+1}\Delta\varepsilon_i^p - Qp_i^{n+1}\Delta p_i) \tag{18}$$

3.2 HIGH-ORDER TVD METHODS

The high order Total Variation Diminishing methods enable to meet both high order of accuracy in smooth regions and a high resolution of discontinuity without any spurious oscillations where shocks arise in the solution. Their strength relies on their ability to introduce a controlled amount of numerical viscosity locally, so that to adapt to the local regularity of the solution. Following [1] and [4], the conservative formula (12) can be rewritten in term of flux-difference splitting, plus some additional flux to reach higher order of accuracy:

$$\mathbf{U}_i^{n+1} = \mathbf{U}_i^n - \frac{\Delta t}{\Delta x}\left(\mathcal{A}^+\mathbf{U}_{i-\frac{1}{2}}^n + \mathcal{A}^-\mathbf{U}_{i+\frac{1}{2}}^n\right) - \frac{\Delta t}{\Delta x}\left(\tilde{\mathbf{F}}_{i+\frac{1}{2}}^n - \tilde{\mathbf{F}}_{i-\frac{1}{2}}^n\right) \tag{19}$$

where $\mathcal{A}^+\mathbf{U}_{i-1/2}^n = \sum_{p=1}^m (\lambda_{i-1/2}^{(p)})^+ \mathcal{W}_{i-1/2}^{(p)}$ and $\mathcal{A}^-\mathbf{U}_{i+1/2}^n = \sum_{p=1}^m (\lambda_{i+1/2}^{(p)})^- \mathcal{W}_{i-1/2}^{(p)}$ are the right-going and left-going fluctuations respectively, provided $\mathbf{U}_{i-1/2}^n = \mathbf{U}_i^n - \mathbf{U}_{i-1}^n$, $\mathcal{W}_{i-1/2}^{(p)} = \alpha_{i-1/2}^{(p)}\mathbf{K}^{(p)}$ are the waves formed of the wave strength coefficient $\alpha_{i-1/2}^{(p)}$ weighting the right eigenvectors $\mathbf{K}^{(p)}$ of the jacobian matrix $\mathbf{A} = \partial\mathbf{f}/\partial\mathbf{u}$, and $(\lambda_{i-1/2}^{(p)})^\pm$ are the characteristic speeds (the eigenvalues of $\mathbf{A}$) travelling rightward or leftward respectively. In addition, $\tilde{\mathbf{F}}_{i+1/2}^n$ and $\tilde{\mathbf{F}}_{i-1/2}^n$ stand for limited additional correction fluxes designed so that the method achieves a high order of accuracy in smooth regions and a high resolution of discontinuity in rough ones. These limited fluxes are expressed as a function of limited waves $\tilde{\mathcal{W}}_{i-1/2}^{(p)} = \tilde{\alpha}_{i-1/2}^{(p)}\mathbf{K}^{(p)}$, $1 \leq p \leq m$:

$$\tilde{\mathbf{F}}_{i-\frac{1}{2}}^n = \frac{1}{2}\sum_{p=1}^m |\lambda_p|\left(1 - \frac{\Delta t}{\Delta x}|\lambda_p|\right)\tilde{\alpha}_{i-1/2}^{(p)}\mathbf{K}^{(p)} \tag{20}$$

These waves are limited based on an upwind ratio $\theta_{i-1/2}^{(p)}$ defined for the $p-$wave as:

$$\theta_{i-1/2}^{(p)} = \frac{\mathcal{W}_{I-1/2}^{(p)}}{\mathcal{W}_{i-1/2}^{(p)}} = \frac{\alpha_{I-1/2}^{(p)}}{\alpha_{i-1/2}^{(p)}} \tag{21}$$

where the index I denotes the upwind interface of that located at $x_{i-1/2}$, that is I equals $i-1$ if $\lambda_{i-1/2}^{(p)} > 0$, $i+1$ if $\lambda_{i-1/2}^{(p)} < 0$. This ratio may be understood as a certain measure of the local regularity of the solution, the $p-$wave strength may thus be limited as a function of this measure:

$$\tilde{\alpha}_{i-1/2}^{(p)} = \phi(\theta_{i-1/2}^{(p)})\alpha_{i-1/2}^{(p)} \tag{22}$$

where $\phi(\theta_{i-1/2}^{(p)})$ is a limiting function. Among many others, Lax-Wendroff is found for $\phi(\theta) = 1$, and for instance Superbee is obtained for $\phi(\theta) = \max(0, \min(1, 2\theta), \min(2, \theta))$.

Implementing a thermo-elastic-plastic material also requires a special elastic-plastic Riemann solver. This is also based on a prediction-correction scheme. First, an elastic trial solution

$(\sigma_{i+1/2})^{\text{trial}}$ is computed at each interface, solution of an elastic Riemann problem consisting of two elastic (discontinuous) waves travelling at speeds $-c_e$ and c_e. Then, this trial stress state is tested against the yield criterion in both grid cells i and $i+1$, being given their respective cumulated plastic strain values (p_i^n, p_{i+1}^n) and temperature values (T_i^n, T_{i+1}^n). In each of these grid cells, either the plastic yield criterion is satified, and then only one elastic wave occurs, or the criterion is violated, and then a plastic wave travelling at speed $\pm c_p$ should be added to the elastic one. In all, the characteristic spectrum solution of the elastic-plastic Riemann problem may consist of (i) two elastic waves if the trial stress state satisfies the yield criterion in both adjacent grid cells, (ii) two elastic waves plus one left or right plastic (discontinuous) wave if the trial stress state has violated the yield criterion in the sole left of right grid cell adjacent to the interface, or (iii) two elastic waves plus two plastic waves if the trial stress state violates the yield criterion in both grid cells i and $i+1$, as shown in figure 1. Notice that the plastic

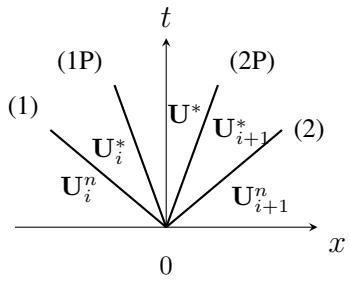

Figure 1: Characteristic structure of the elastic-plastic Riemann problem.

waves here involved in the solution of the elastic-plastic Riemann problem are actually strong discontinuous waves since a linear hardening is considered in this work. A nonlinear hardening would yield weak discontinuous plastic centered rarefaction waves: this case will be treated in a latter work.

It remains to compute the strength $\alpha_{i+1/2}^{(p)}$ of each of these waves. This is based on the decomposition of $\mathbf{U}_{i+1/2}$ on the eigenbasis of the jacobian matrix $\mathbf{A} = \partial \mathbf{f} / \partial \mathbf{u}$:

$$\mathbf{U}_{i+\frac{1}{2}} = \mathbf{U}_{i+1}^n - \mathbf{U}_i^n = \sum_{p=1}^{m} \alpha_{i+1/2}^{(p)} \mathbf{K}^{(p)} \tag{23}$$

The strength of elastic waves are first computed since the stresses in areas $\mathbf{U}_i^*$ and $\mathbf{U}_{i+1}^*$ are known and equal to the respective tensile yield stresses. Then, the strengths of plastic waves are computed by forming a system of equations with the two remaining waves. For example, if plasticity occurs from both sides, the two plastic wave strength are computed by:

$$\left[\mathbf{K}^{(1P)}\,,\,\mathbf{K}^{(2P)}\right] \begin{bmatrix} \alpha_{i+1/2}^{(1P)} \\ \alpha_{i+1/2}^{(2P)} \end{bmatrix} = \mathbf{U}_{i+1}^n - \mathbf{U}_i^n - \alpha_{i+1/2}^{(1)} \mathbf{K}^{(1)} - \alpha_{i+1/2}^{(2)} \mathbf{K}^{(2)} \tag{24}$$

The fluctuations $\mathcal{A}^+ \mathbf{U}_{i+1/2}^n$ and $\mathcal{A}^- \mathbf{U}_{i+1/2}^n$ are then computed, and the unknowns $\mathbf{U}_i^{n+1}$ are hence updated at time t_{n+1} through the formula (19). The thermomechanical coupling is treated as discussed in section 3.1.

4 SUDDEN UNLOADING OF STRONG-DISCONTINUOUS LOADING WAVE IN A LINEAR HARDENING BAR

We consider a semi-infinite bar made of a linear hardening material, in an initial natural state, suddenly loaded on its left side at time $t = 0$ with a constant tensile stress value σ^* sufficiently large to deform the bar plastically. After time t_u, the applied load is suddenly released to zero. The analytical solution of this problem can be found in [8], and is summarized in figure 2. A

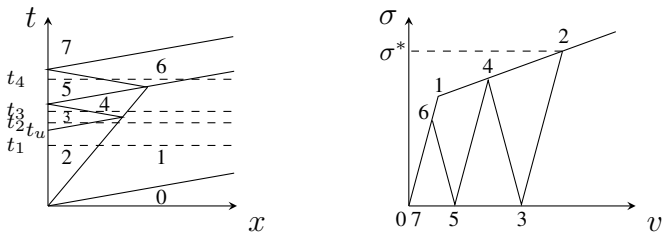

Figure 2: Analytical solution of a semi-infinite bar suddenly plastically loaded then unloaded on its end, plotted with two strain strong-discontinuities here.

stationary strong-discontinuous strain interface is formed at each unloading cycle, the righward plastic wave being weakened until it disappears. Introducing the parameter β defined by:

$$\beta = \frac{c_e + c_p}{c_e - c_p} > 1 \tag{25}$$

the length of the $(n+1)$th stationary strain-discontinuous interfaces, l_{n+1}, and its stress associated are given by:

$$\begin{aligned} l_{n+1} &= \beta l_n \\ \sigma_{2(n+1)} &= \frac{\sigma_{2n}}{\beta} \end{aligned} \qquad (n = 1, 2, \ldots) \tag{26}$$

where l_n the length of the nth stationary strain-discontinuous interfaces and σ_{2n} the stress associated.

4.1 COMPARISON WITH THE FINITE ELEMENT METHOD FOR AN ELASTIC-PLASTIC MATERIAL

The numerical results obtained for a steel (see table 1 for numerical values of parameters) with the Lax-Wendroff and the second-order TVD Superbee finite volume methods are compared here to the analytical solution of this test case and to the results obtained with the finite element method coupled with an explicit time integrator. The constitutive equations in the latter solution is integrated with a radial return algorithm [9], and the solution is computed within a larger domain than that shown in figures 3 to mimic a semi-infinite bar. For the finite volume solutions, transmittive boundary conditions have been set on the right side of the bar.

Both the stress and plastic strain fields are compared at instants t_1, t_2, t_3 and t_4 (see figure 2), in figures 3. When the bar is loaded, an elastic precursor travels at the elastic sound speed (see figure 3(a)), followed by a plastic wave. Since the Courant number has been set at one, the three numerical methods fit perfectly the analytical solution. However, the plastic wave travels slower, numerical oscillations appears for the Finite Element (the largest ones) and Lax-Wendroff solutions. For the latter one, this is due to the fact that Lax-Wendroff is not a monotone

$E = 2 \cdot 10^{11}$ Pa	$\sigma_0 = 400 \cdot 10^6$ Pa	$L = 6$ m
$\rho = 7800$ kg.m^{-3}	$A = 4$	number of grid cells/elements = 100
$C = 450$ J.kg^{-1}.K^{-1}	$T_0 = 293$ K	$t_u = 1.2 \cdot 10^{-3}$ s
$Q = 10 \cdot 10^9$ Pa	$\sigma^* = 900 \cdot 10^6$ Pa	

Table 1: Numerical values of parameters

method nor a TVD one. Moreover, the Finite element solution overestimates the plastic strain value closed to the boundary, though reduces to the right values when it departs. Superbee achieves the best resolution of the plastic wave on five cells here.

Then, the prescribed load is released to zero, and an unloading wave pursues the forerunning plastic loading disturbance (see figure 3(b)). Strong oscillations appears at integration points within the unloaded area in the Finite Element solution. Many solutions can be used to reduce these oscillations, among others (i) unload in two time steps rather than in one, (ii) reaverage at integration points the stress moved at nodes using the finite element shape functions or (iii) adding some additional numerical viscosity. Superbee achieves a proper elastic unload, superposed with the analytical solution, while Lax-Wendroff is not so bad.

When the unloading wave catches up with the plastic wave, a discontinuity of the (plastic) strain appears at this point due to the strain history difference on both sides (see figure 3(c)). Thus, a stationary discontinuous interface is generated, as well as internal reflective waves, so that the plastic strain continues to propagate rightward, but with a smaller value. The resolution of these two plastic strain fronts is quite close for these three numerical methods.

A second unload disturbance is required here to stop the progession of plastic strain (see figure 3(d)). The stress front is poorly solved by the finite element method, Lax-Wendroff has also difficulties with the left front. Only Superbee gives acceptable results after several reflexions of plastic waves.

4.2 COMPARISON WITH THE FINITE ELEMENT METHOD FOR A THERMO-ELASTIC-PLASTIC MATERIAL

The thermomechanical coupling is here added, with numerical parameters listed in table 1. Since on the one hand a linear hardening is considered in this work, and the other hand the thermal part influences the mechanical one through the sole yield stress, the plastic sound speed is not affected by the temperature here, but the stress and the plastic strain actually depend on the temperature. With the numerical values of parameters listed in table 1, the stress does not change much with respect to figure 3 at the beginning, though more after many wave reflexions. The change in plastic strain is much pronounced. The thermo-elastic-plastic (TEP) numerical solutions are plotted in figure 4, and the plastic strains superposed with the (isothermal) elastic-plastic (EP) analytical solution to observe the effect of the thermomechanical coupling. The decrease of the tensile yield stress through thermal softening leads to an increase of the plastic flow, and hence to an increase of temperature (figures 4(a) and 4(b)). Recall that adiabatic conditions have been assumed so that no conduction effects are here accounted for. This explains why the temperature and plastic strain profiles are similar.

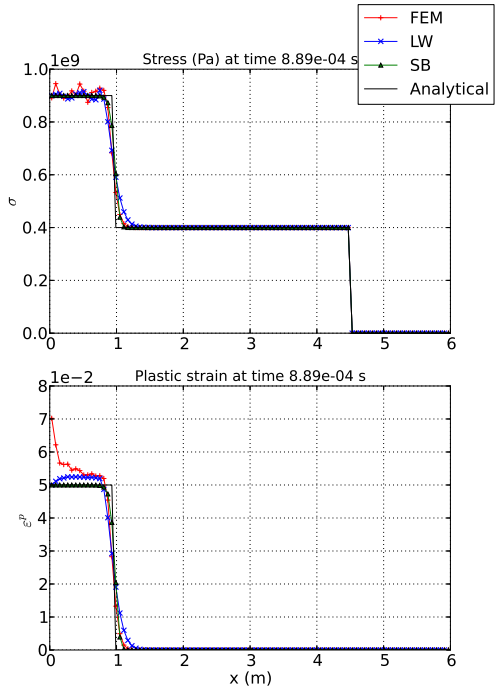

(a) Time $t_1 = 8.89 \cdot 10^{-4}$ seconds.

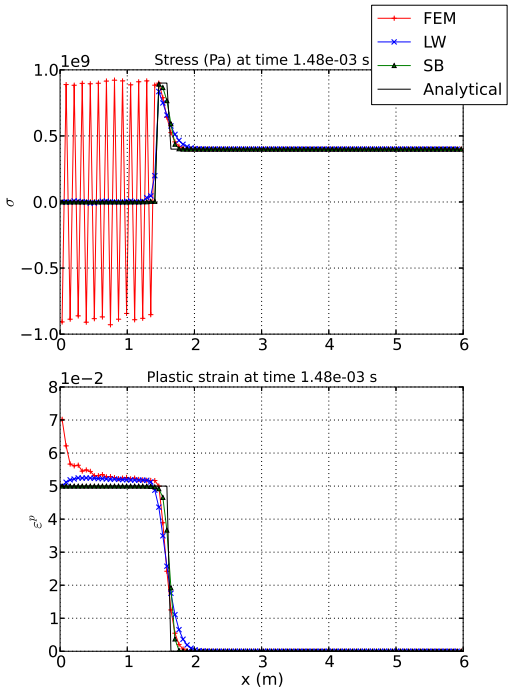

(b) Time $t_2 = 1.48 \cdot 10^{-3}$ seconds.

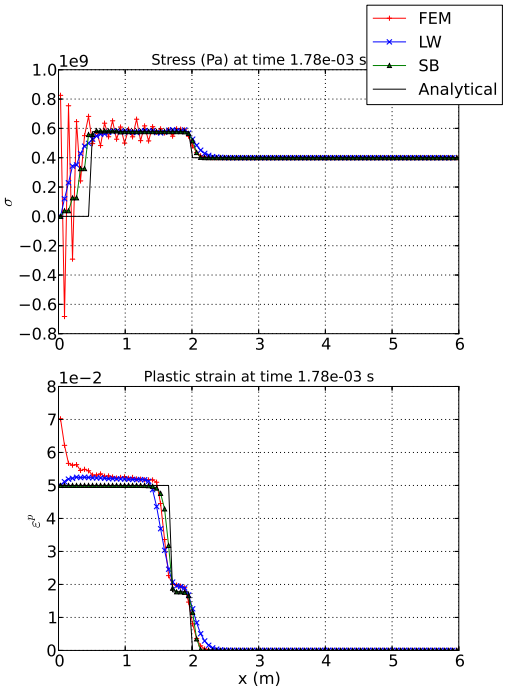

(c) Time $t_3 = 1.78 \cdot 10^{-3}$ seconds.

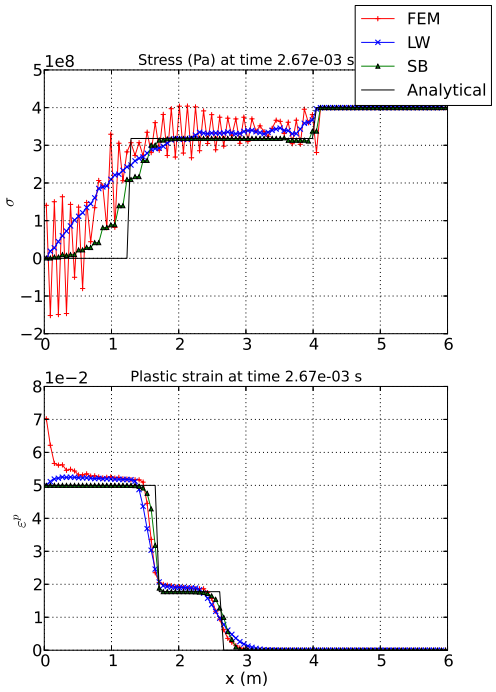

(d) Time $t_4 = 2.67 \cdot 10^{-3}$ seconds.

Figure 3: Comparison of the analytical, Finite Element (FEM), Lax-Wendroff (LW) and Superbee (SB) stress and plastic strain fields at different times.

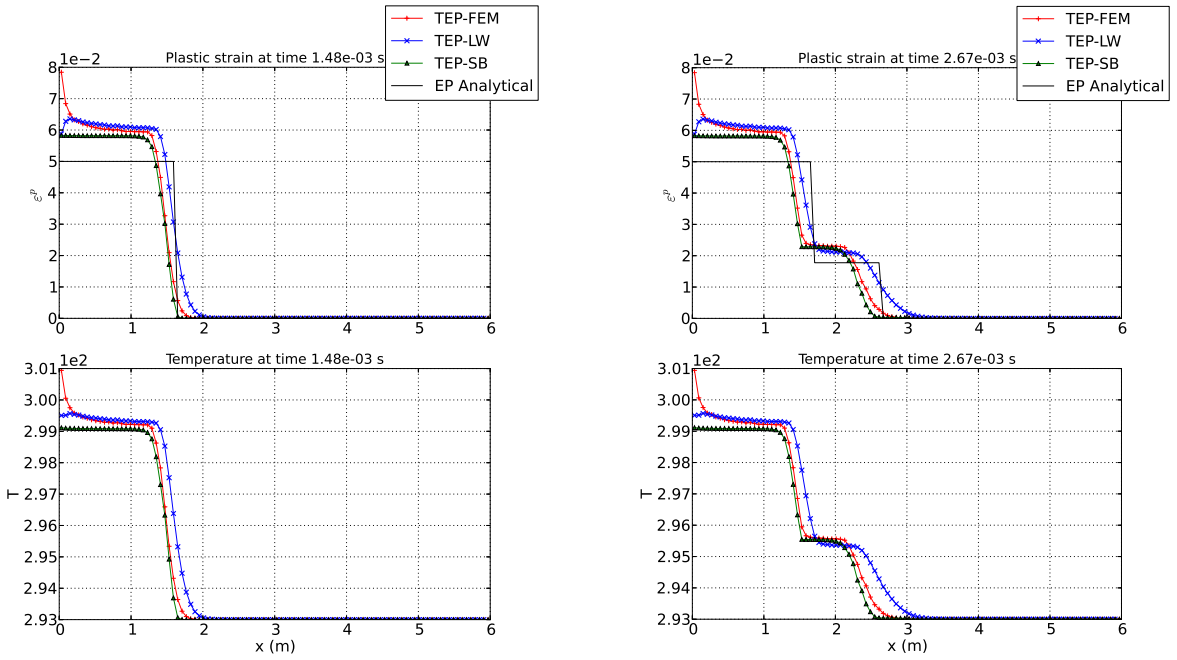

(a) Time $t_2 = 1.48 \cdot 10^{-3}$ seconds.

(b) Time $t_4 = 2.67 \cdot 10^{-3}$ seconds.

Figure 4: Comparison of the analytical, Finite Element (FEM), Lax-Wendroff (LW) and Superbee (SB) plastic strain and temperature fields at different times.

5 CONCLUSIONS

In this work, two schemes of the finite volume methods (namely the Lax-Wendroff and the Superbee TVD limiter) have been implemented for the numerical simulation of impacts on thermo-elastic-plastic bars. These methods were tested against an analytical solution and the finite element method on a test case involving strong discontinuous waves. The Superbee TVD limited solution has been shown to be the best in term of accuracy, so that it improves both the track of the shock wave path, even after many reflexions of waves, and the computation of plastic strains and temperature.

REFERENCES

[1] R. Leveque, *Finite volume methods for hyperbolic problems.* Cambridge University PressMcGraw Hill, 2002.

[2] C. Lee, A. Gil, J. Bonet, (2013). Development of a cell centred upwind finite volume algorithm for a new conservation law formulation in structural dynamics. *Computers and Structures*, **118**, 13–38, 2013.

[3] G. Miller, P. Collela, A high-order eulerian Godunov method for elastic-plastic flow in solids. *Journal of Computational Physics*, **167**, 131–176, 2001.

[4] T. Fogarty. Finite volume methods for acoustics and elasto-plasticity with damage in a heterogeneous medium. PhD thesis, University of Washington, 2001.

[5] P. Barton, R. Deiterding, D. Meiron, D. Pullin, Eulerian adaptive finite-difference method for high-velocity impact and penetration problems. *Journal of Computational Physics*, **240**, 76–99, 2013.

[6] A.L. Ortega, M. Lombardini, D. Pullin, D. Meiron, Numerical simulation of elastic-plastic solid mechanics using an eulerian stretch tensor approach and HLLD Riemann solver. *Journal of Computational Physics*, **257**, 414–441, 2014.

[7] M. Aguirre, A. Gil, J. Bonet, C. Lee, An upwind vertex centred finite volume solver for lagrangian solid dynamics. *Journal of Computational Physics*, **300**, 387–422, 2015.

[8] L. Wang, *Foundations of stress waves.* Elsevier, 2011.

[9] J.C. Simo, T.J.R. Hughes. Computational Inelasticity. Springer, 1997.